arXiv:1409.0237v1 [astro-ph.SR] 31 Aug 2014

OT J075418.7+381225 and OT J230425.8+062546: Promising Candidates for the Period Bouncer

Chikako Nakata,[1*] Taichi Kato,[1] DaisakuNogami,[1] Elena Pavlenko,[2,1] Tomohito Ohshima,[1] Enrique de Miguel,[3,4] William Stein,[5] Kazuhiko Siokawa,[7] Etienne Morelle,[6] Hiroshi Itoh,[8] Pavol A. Dubovsky,[9] Igor Kudzej,[9] Hiroyuki Maehara,[10] Arne Henden,[11] William N. Goff,[12] Shawn Dvorak,[13] Oksana Antonyuk,[2] Eddy Muyllaert,[14]

[1] *Department of Astronomy, Kyoto University, Kyoto 606-8502*

[*] *nakata@kusastro.kyoto-u.ac.jp*

[2] *Crimean Astrophysical Observatory, 98409, Nauchny, Crimea, Ukraine*

[3] *Departamento de Física Aplicada, Facultad de Ciencias Experimentales, Universidad de Huelva, 21071 Huelva, Spain*

[4] *Center for Backyard Astrophysics, Observatorio del CIECEM, Parque Dunar, Matalascañas, 21760 Almonte, Huelva, Spain*

[5] *6025 Calle Paraiso, Las Cruces, New Mexico 88012, USA*

[6] *9 rue Vasco de GAMA, 59553 Lauwin Planque, France*

[7] *Moriyama 810, Komoro, Nagano 384-0085*

[8] *VSOLJ, 1001-105 Nishiterakata, Hachioji, Tokyo 192-0153*

[9] *Vihorlat Observatory, Mierova 4, Humenne, Slovakia*

[10] *Kiso Observatory, Institute of Astronomy, School of Science, The University of Tokyo, 10762-30, Mitake, Kiso-machi, Kiso-gun, Nagano 397-0101, Japan*

[11] *American Association of Variable Star Observers, 49 Bay State Rd., Cambridge, MA 02138, USA*

[12] *13508 Monitor Ln., Sutter Creek, California 95685, USA*

[13] *Rolling Hills Observatory, 1643 Nightfall Drive, Clermont, Florida 34711, USA*

[14] *Vereniging Voor Sterrenkunde (VVS), Moffelstraat 13 3370 Boutersem, Belgium*

(Received 201 0; accepted 201 0)

Abstract

We report on photometric observations of two dwarf novae, OT J075418.7+381225 and OT J230425.8+062546, which underwent superoutburst in 2013 (OT J075418) and in 2011 (OT J230425). Their mean period of the superhump was 0.0722403(26) d (OT J074518) and 0.067317(35) d (OT J230425). These objects showed a very long growing stage of the superhump (stage A) and a large period decrease in stage A-B transition. The long stage A suggests slow evolution of the superhump due to very small mass ratios of these objects. The decline rates during the plateau

phase in the superoutburst of these objects were lower than those of SU UMa-type DNe with a similar superhump period. These properties were similar to those of SSS J122221.7−311523, the best candidate for the period bouncer. Therefore, these two DNe are regarded as good candidates for the period bouncer. We estimated the number density of period bouncers roughly from our observations in the recent five years. There is a possibility that these WZ Sge-type dwarf novae with unusual outburst properties can account for the missing population of the period bouncer expected from the evolutionary scenario.

Key words: accretion, accretion disks — stars: novae, cataclysmic variables — stars: dwarf novae — stars: individual (OT J075418.7+381225) — stars: individual (OT J230425.8+062546)

1. Introduction

Cataclysmic variables (CVs) are binary star systems composed of a white dwarf (primary) and a secondary which is typically a late-type main sequence star. The secondary fills its Roche lobe and matter falls down toward the primary spilling over from the inner lagrangian point (L_1 point).

Dwarf novae (DNe) are one of subtypes of CVs. DNe undergo recurring outbursts. The outburst lasts for an order of days to weeks, during which their brightness increases by 2 to 5 mag. The outburst results from a release of gravitational energy which is caused by a sudden increase of the mass accretion rate by the thermal instability in the disk.

SU UMa-type dwarf novae are a subclass of DNe. They have relatively short orbital periods (1–2 hrs, near to the period minimum) and occasional "superoutbursts" that are brighter and have longer durations than the normal outbursts. The superhumps are believed to result from the tidal instability that is triggered when the disk radius reaches the critical radius for the 3 : 1 resonance (Osaki 1989). WZ Sge-type DNe are a subgroup of SU UMa-type DNe. They have particularly short orbital periods and show infrequent large-amplitude superoutbursts [for general properties of WZ Sge-type DNe, see e.g. Bailey (1979); Downes (1990); Kato et al. (2001)]. During the superoutbursts, superhumps, periodic light variations whose period is a few percent shorter than the orbital period, are seen. The superhump periods vary through a course of three stages: the first is the stage A with a longer superhump period, the middle is the stage B with a systematically varying period, and the final is the stage C with a shorter superhump period (Kato et al. 2009).

According to the standard evolutionary theory of CVs, the mass transfer from the secondary starts when the secondary fills its Roche lobe. The orbital period $P_{\rm orb}$ is longer when a CV is formed and the system evolves with $P_{\rm orb}$ becoming shorter. Once its $P_{\rm orb}$ reaches

the period minimum, the secondary becomes oversized for its mass as a result of deviation from thermal equilibrium or becomes a brown dwarf which cannot maintain in hydrogen burning. After this point, the system evolves toward longer period and it is usually called "period bouncer" [see e.g. Knigge et al. (2011) and references there in, for standard evolutionary theory of CVs].

The study about the period bouncers ought to play a vital role in resolving the problems about the terminal evolution of CVs, since it is said that Kolb (1993) estimated that 70% of CVs should have passed the period bounce. The candidates for the period bouncer, however, have hardly been discovered. One of the reasons is that CVs become much fainter as they approach the period minimum (Patterson 2011). Littlefair et al. (2006) also gave a great impact on the problem about the missing population in the CVs. They confirmed the secondary in the eclipsing short-period CV SDSS 103533.03+055158.4 was a brown dwarf, which suggests that the system is the period bouncer. Recently, Littlefair et al. (2008) discovered more three systems which have a brown dwarf secondary with high-speed three-color photometry. In photometric research in the period bouncers, until recently, WZ Sge-type DNe with multiple rebrightenings such as EG Cnc have been considered to be a good candidate for the period bouncer (Patterson et al. 1998). Recently, Kato, Osaki (2013) succeeded in interpreting the variation of the superhump period around the stage A and developed a new dynamical method to estimate the binary mass ratios ($q \equiv M_2/M_1$) only from the stage A superhump observations and the orbital period. Using this new method, it become evident that many of WZ Sge-type DNe with multiple rebrightenings do not likely have low mass ratios as estimated in EG Cnc (Nakata et al. 2013). After this suggestion, a new candidate for the period bouncer was discovered; Kato et al. (2013b) reported SSS J122221.7−311523 (hereafter SSS J122221), a transient discovered by Catalina Real-time Transient Survey (CRTS, Drake et al. 2009) Siding Spring Survey (SSS), had a very small mass ratio $q = 0.045$ and long orbital period [possible period of 0.075879(1) d]. They also revealed a characteristic property of SSS J122221 that stage A superhumps lasted for long time.

In this paper, we present two DNe which are similar in some properties to SSS J122221. OT J075418.7+381225 (hereafter OT J075418) was detected by CRTS as CSS 130131 on 2013 January 31. The quiescent counterpart was g=22.8 mag SDSS J075418.72+381225.2. The observed superhumps with a period of 0.07 d were suggestive of an SU UMa-type dwarf nova (vsnet-alert 15355). OT J230425.8+062546 (hereafter OT J230425) was originally reported as a possible nova discovered by Hideo Nishimura on 2010 December 29 at 13.7 mag (Nakano et al. 2011). The quiescent counterpart was g=21.1 mag SDSS J230425.88+062545.6. After this, it was suggested to be a dwarf nova on the basis of the color of the SDSS counterpart (vsnet-alert 12548). Subsequent observations detected the presence of superhumps with an amplitude of 0.06 mag (A. Arai, vsnet-alert 12563). Although observations and analysis of OT J230425 were already reported as a summary form in Kato et al. (2012), we present a new interpretation of

this object in this paper.

This paper is structured as follows. Section 2 briefly shows a log of observations and our analysis method. Sections 3 and 4 deal with the results of the observations of OT J075418 and OT J230425, respectively. Section 5 discusses the results.

2. Observation and Analysis

Tables 2 and 3 show the logs of photometric observations. All the observation times were written in barycentric Julian days (BJDs). To correct zero-point of data differences between different observers, we added a constant to each observer's data.

The phase dispersion minimization (PDM) method (Stellingwerf 1978) was used in a period analysis. In subtracting the global trend of the light curve, we subtracted smoothed light curve obtained by locally-weighted polynomial regression (LOWESS, Cleveland 1979) before making the PDM analysis. The 1-σ error of the best estimated period by the PDM analysis was determined by the methods in Fernie (1989), Kato et al. (2010).

A variety of bootstrapping was used to estimating the robustness of the result of PDM. We analyzed about 100 samples which randomly contain 50% of observations, and performed PDM analysis for these samples. The result of bootstrap is displayed as a form of 90% confidence intervals in the resultant θ statistics.

3. OT J075418.7+381225

3.1. Overall Light Curve

Figure 1 shows the overall light curve of OT J075418. After a precursor outburst (marked with an arrow in figure 1), the superoutburst started on BJD 2456326. The early rise was well observed during BJD 2456326–2456327. The superoutburst lasted with a slow decline for at least 30 d. In the middle part of the superoutburst (BJD 2456341–2456345), there were no observations. On BJD 2456346, observations were resumed and they showed a small rise of brightness. On BJD 2456352, there was a rapid brightening. This phenomenon was confirmed by using different comparison stars. It may have been an interesting phenomenon that we could not explain theoretically. It, however, may have been an artifact, since the observing condition was very bad due to clouds and the moon.

3.2. Superhumps

Figure 2 shows that a period analysis using the Phase Dispersion Minimization (PDM) method (Stellingwerf 1978) indicated the presence of a period of 0.072218(3) d during stage A (BJD 2456328–2456341) and 0.070758(6) d during stage B (BJD 2456345–2456355). The mean profile of stage A and stage B superhumps are also shown in lower part of figure 2. The amplitude of the superhumps during stage B is larger than that during stage A.

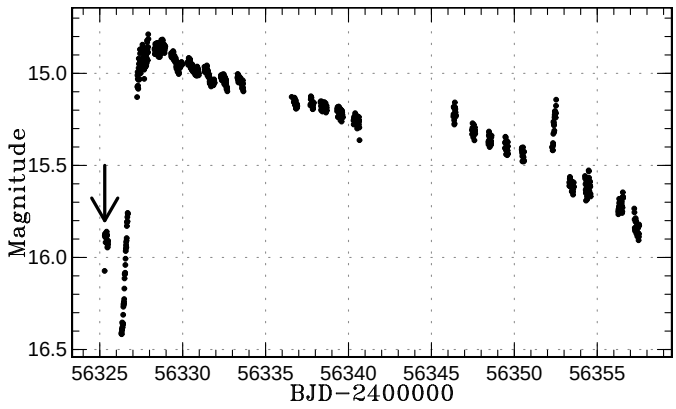

Fig. 1. Overall light curve of OT J075418. The data were binned to 0.01 d. The arrow indicates the precursor.

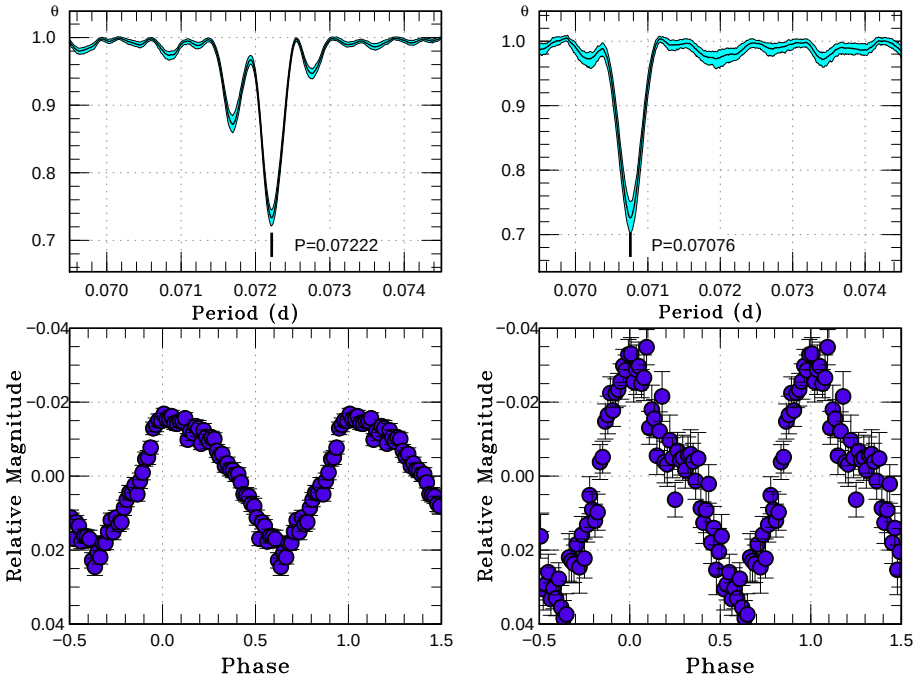

Fig. 2. Superhumps in OT J075418 (BJD 2456328–2456358). (Left upper): θ diagram of our PDM analysis of stage A superhumps (BJD 2456328–2456341). (Left lower): Phase-averaged profile of stage A superhumps. (Right upper): θ diagram of our PDM analysis of stage B superhumps (BJD 2456345–2456355). (Right lower): Phase-averaged profile of stage B superhumps.

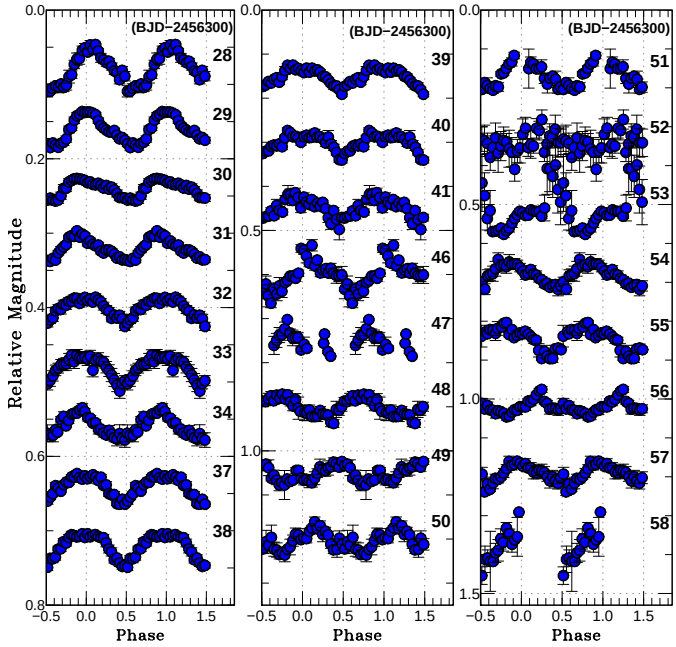

Fig. 3. Nightly variation of the profile of superhumps in OT J075418.

Figure 3 shows the nightly variation of the profile of superhumps. The amplitude of superhumps was 0.03–0.06 mag, smaller than in typical SU UMa-type DNe.

We determined the times of maxima of ordinary superhumps as in the way described in Kato et al. (2009). The resultant times are listed in table 4.

The $O-C$ curve of OT J075418 is shown in figure 4. The very long stage A ($30 \leq E \leq 220$) and stage B ($E \geq 280$) are seen. Although the data when the stage A-B transition took place cannot be estimated precisely because of lack of observations, it occurred between BJD 2456342 and 2456346. In the stage A, superhumps with a mean period of $P_{\rm sh}$ =0.0722179(32) d and the time derivative of the superhump period $P_{\rm dot}$ ($= \dot{P}/P$) =+3.6(0.7) $\times 10^{-5}$ s/s were recorded. In the stage B, superhumps with a mean period of 0.0707581(58) d and $P_{\rm dot}$ of $-2.4(0.5) \times 10^{-5}$ s/s were recorded.

3.3. Two-dimensional Lasso Analysis

The least absolute shrinkage and selection operator (Lasso) method was introduced by Kato, Uemura (2012). This method has been proven to be very effective in separating closely spaced periods and has extended to two-dimentional power spectra (Osaki, Kato 2013; Kato, Maehara 2013).

A two-dimensional Lasso analysis of OT J075418 data is shown in figure 5. A major change of frequency from $\sim$ 13.85 c/d to $\sim$ 14.1 c/d can be seen between BJD 2456341 and 2456345. It suggests that change coincided with the timing when the stage A-B transition occurred. During the stage A (BJD 2456328–2456341), the frequency become lower. In contrast, it shows a tendency to become higher in the stage B (BJD 2456345–2456355).

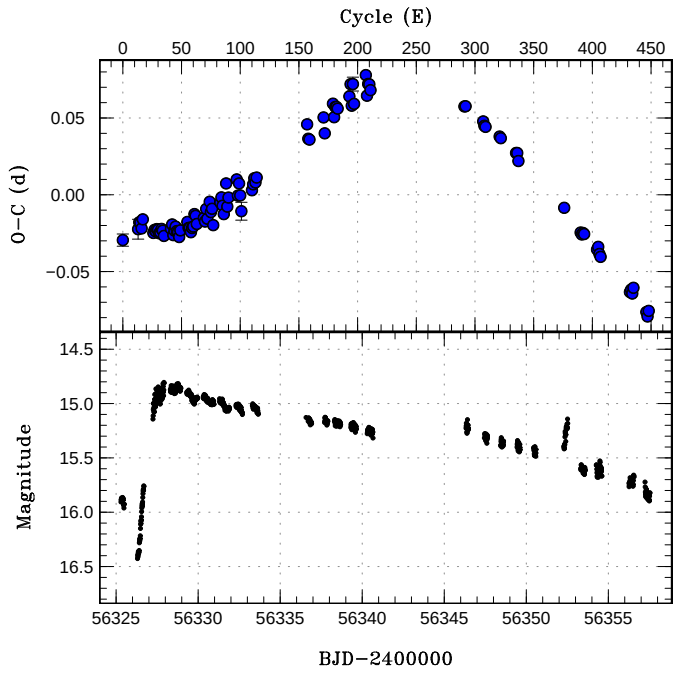

Fig. 4. (Upper:) The $O-C$ curve of OT J075418. A ephemeris of BJD 2456325.4414 + 0.0716368E was used to draw this figure. (Lower:) Overall light curve, the same as in figure 1. The horizontal axis in units of BJD and the cycle number is common in both of upper and lower panels.

4. OT J230425.8+062546

4.1. Overall light curve

Figure 6 shows the overall light curve of OT J230425. This object was discovered on December 29 in 2011 (BJD 2455559) with the recorded possible maximum brightness of $V = 13.72$. The early rise was missed. The superoutburst lasted for about 25 d. The light curve showed a slow decline until BJD 2455575. After BJD 2455578, it declined faster.

4.2. Superhumps

During BJD 2455563–2455585, superhumps with amplitudes of 0.03–0.07 mag were present. A period analysis using all the data indicated that the mean superhump period was 0.067317(35) d. The PDM analysis of all superhumps was shown in Kato et al. (2012).

A period analysis indicated a change of the period from 0.067245(17) d during stage A (BJD 2455563–2455572) to 0.066351(12) d during stage B (BJD 2455571–2455585) (figure 7). The mean profile of stage A and stage B superhumps are also shown in the lower panels of figure 7. Figure 8 shows the nightly variation of the profile of superhumps. The maximum amplitude of superhumps was seen around BJD 2455571.

Displayed in top right panel of figure 7, there was a possible period which is shorter than the indicated period 0.066351(12) d. It was suggested that the period was a possible orbital period of 0.06589(1) d. Assuming 0.06589(1) d to be the orbital period, the new method using

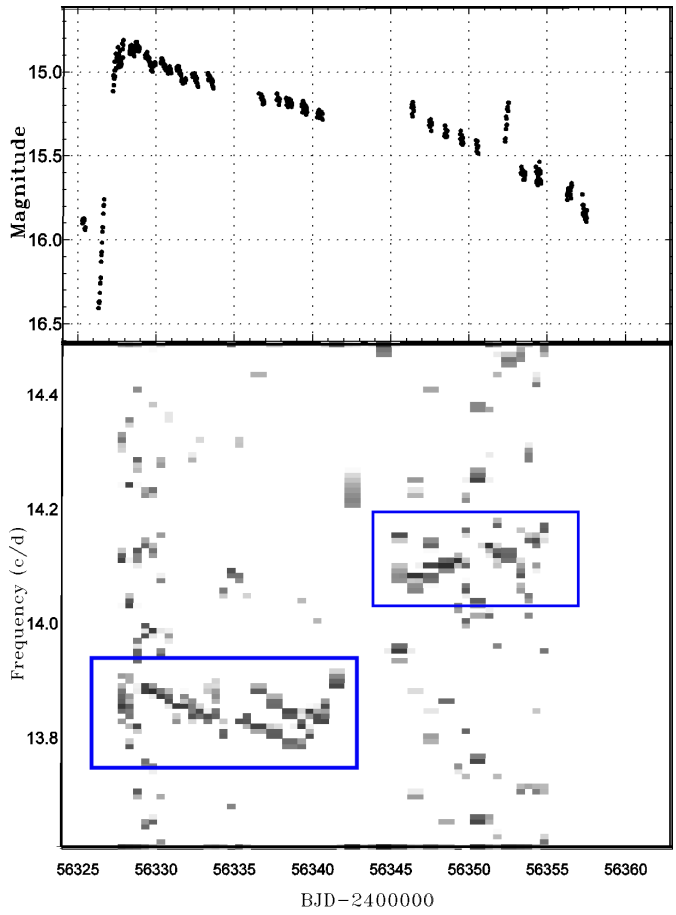

Fig. 5. Two-dimensional Lasso period analysis of OT J075418. (Upper:) Overall light curve binned to 0.01 d, the same as figure 1. (Lower:) Result of two-dimensional Lasso analysis (5 d window, 0.5 d shift and $\log\lambda = -8.5$). The appearance of the stage A and stage B frequency is boxed.

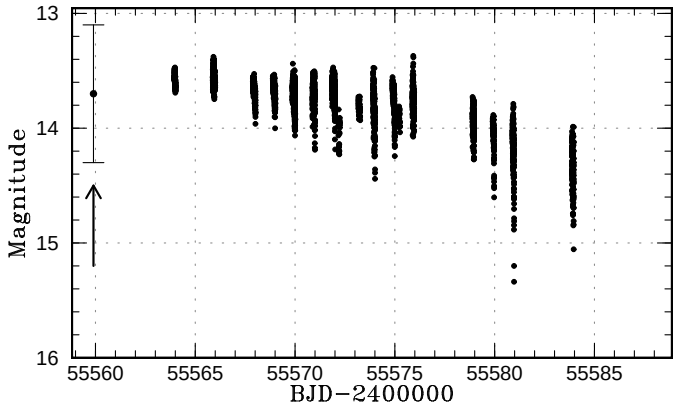

Fig. 6. Overall light curve of OT J230425. The data were binned to 0.01 d. The arrow indicates the discovery of the superoutburst (Nakano et al. 2011).

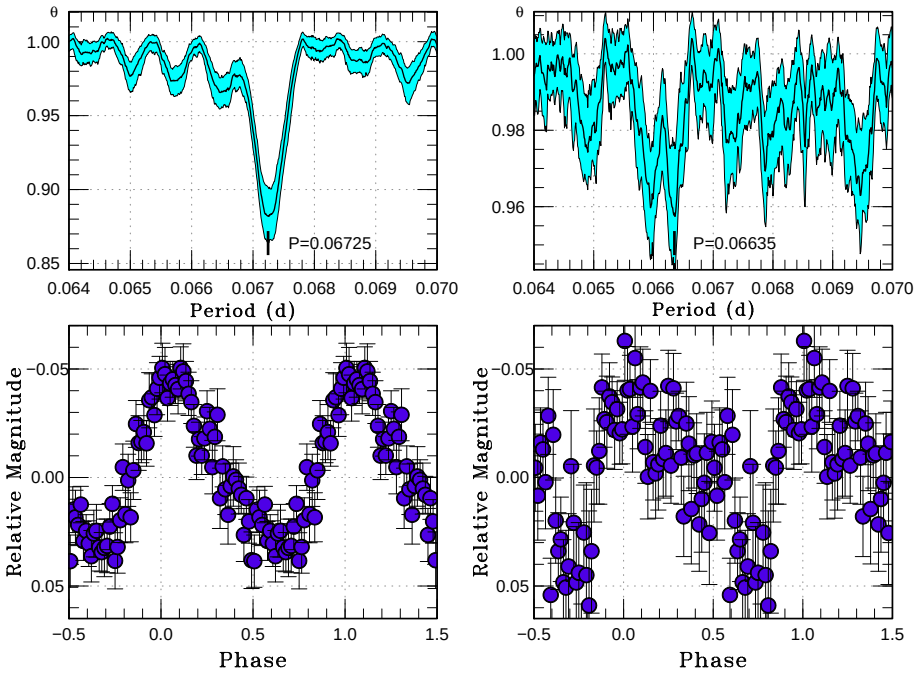

Fig. 7. Superhumps in OT J230425 (BJD 2455563–2455585). (Left upper): θ diagram of our PDM analysis of stage A superhumps (BJD 2455563–2455572). (Left lower): Phase-averaged profile of stage A superhumps. (Right upper): θ diagram of our PDM analysis of stage B superhumps (BJD 2455571–2455585). (Right lower): Phase-averaged profile of stage B superhumps.

stage A superhumps (Kato, Osaki 2013) implies $q = 0.053(1)$. It suggests that OT J230425 is a good candidate for the period bouncer.

Figure 9 exhibits an $O-C$ curve of OT J230425 (filled circles), compared with $O-C$ curve of OT J075418 exhibited in figure 4 (filled squares). The resultant times of OT J230425 are listed in table 5. The $O-C$ curve of OT J230425 is very similar to that of OT J075418. The very long stage A ($E \leq 123$) and the subsequent stage B ($E \geq 118$) are seen. The stage A-B transition occurred around BJD 2455572. The periods of superhumps in stage A and stage B were 0.067194(30) d and 0.066281(63) d, respectively. The $P_{\rm dot}$ in stage B was $-3.9(2.4) \times 10^{-5}$ s/s.

5. Discussion

5.1. Decrease of Superhump Period between Stage A and B

The $O-C$ curves of OT J075418 and OT J230425 (figures 4 and 9) suggest a very long stage of increasing $O-C$ values (or a long period) and certain stage transition in the middle of the superoutbursts. Kato et al. (2009) argued that the superhump period usually decreases by 1.0–1.5% at the stage A-B transition and by $\sim 0.5\%$ at the stage B-C transition. The fractional period decrease at the transition was $\sim 2.0\%$ in OT J075418 and $\sim 1.4\%$ in OT J230425. This large variation in frequency of OT J075418 can be clearly seen in figure 5. Since they were too

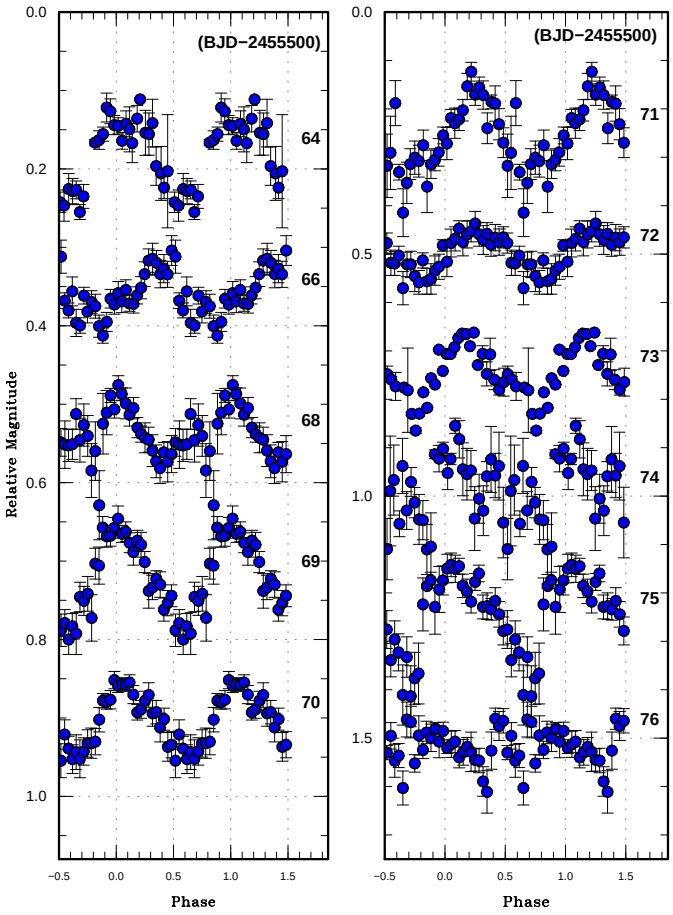

Fig. 8. Nightly variation of the profile of superhumps in OT J230425.

large for the stage B-C transition, we regard this transition as the stage A-B transition.

The disk precession results mainly from the effects of direct axisymmetric tidal potential from the secondary, secondarily from the gas pressure in the eccentric mode and resonant wave stress (Lubow 1992). Although the tidal potential produces a net prograde precession, the gas pressure effect produces a retrograde contribution and decreases the precession rate. Murray (2000) gave the hydrodynamical precession ω in terms of the dynamic precession ($\omega_{\rm dyn}$) and the pressure contribution to the precession ($\omega_{\rm pres}$):

$$\omega = \omega_{\rm dyn} + \omega_{\rm pres}. \quad (1)$$

Note that $\omega_{\rm pres}$ is a negative value according to its retrograde contribution. The ratio $\omega_{\rm pres}/\omega_{\rm orb}$ corresponds to the fractional decrease of the superhump period between stage A and B, where $\omega_{\rm orb}$ is the orbital frequency. Therefore, it is possible that the large decrease of the superhump period between stage A and B indicates a large pressure contribution.

5.2. Slow Evolution of Superhumps

The duration of the stage A reflects the growth time of the 3 : 1 resonance. As shown in subsections 3.2 and 4.2, it took ~ 190 (OT J075418) and ~ 120 superhump cycles (OT

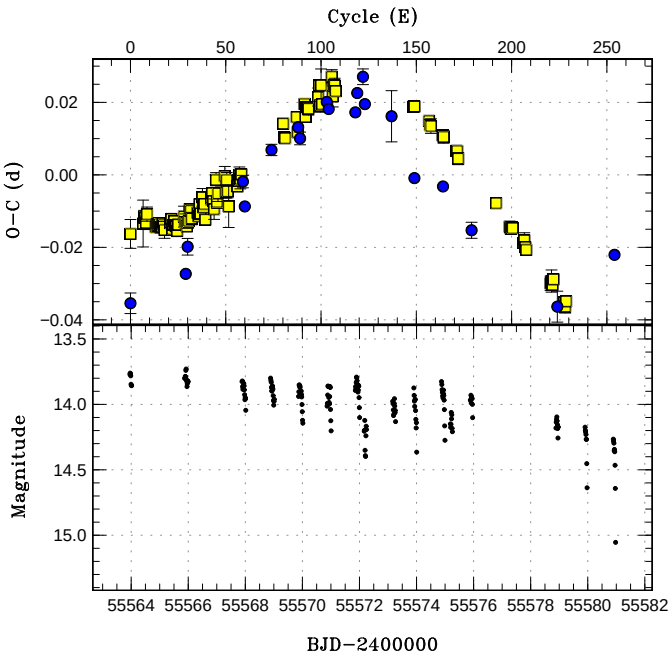

Fig. 9. (Upper:) $O-C$ curve of OT J230425, compared with that of OT J075418. Filled circles and filled squares represent $O-C$ diagram of OT J230425 and that of OT J075418, respectively. To fit two curves, the $O-C$ diagram of OT J075418 was shifted. An ephemeris of BJD 2455565.925 + 0.06695E was used to draw this figure. (Lower:) Light curve of OT J230425, the same as in figure 6.

J230425), respectively to fully develop the 3 : 1 resonance. Considering absence of observation right after discovery of OT J230425, the growth time of the 3 : 1 resonance may be even longer in OT J230425. This long duration of the stage A suggests very small mass ratios q of these objects because the growth time of the 3 : 1 resonance is expected to be inversely proportional to q^2 (Lubow 1991). The duration of the stage A of these objects was 4–8 times longer than those of typical SU UMa-type DNe having short orbital periods of ~ 0.06 d and mass ratios of 0.10–0.15 (Kato et al. 2009). The mass ratios of these objects can be estimated to be 2–3 times smaller, suggesting possible mass ratios ~ 0.05. Despite the possible very small mass ratios, the orbital periods of these objects, which are estimated to be less than 1 % shorter than their superhump periods, are longer than that of typical short-period SU UMa ($P_{\rm orb} \sim 0.06$ d). This supports a hypothesis that these objects are candidates for the period bouncer.

5.3. Slow Fading Rate

During the superoutburst of SU UMa-type dwarf novae, an almost exponential, slow decline phase exists, which is called the plateau phase. Osaki (1989) derived the time scale of this slow fading as follows.

$$t_{\rm d} \simeq 8.14{\rm d} R_{\rm d,10}^{0.4} \alpha_{0.3}^{-0.7}, \tag{2}$$

where $R_{\rm d,10}$ is the disk radius in a unit of 10^{10} cm and $\alpha_{0.3} = \alpha_{\rm hot}/0.3$, respectively ($\alpha_{\rm hot}$

represents the disk viscosity in the hot state). Kato et al. (2014a) suggested that $\alpha_{\rm hot}$ in candidates for the period bouncer that show slow fading rate is probably smaller than in higher-q systems. In addition to this, the radius of the 3 : 1 resonance can be formulated in terms of q:

$$r_{3:1} = 3^{(-2/3)}(1+q)^{-1/3}. \tag{3}$$

A small q, thus, produces a large radius of the 3 : 1 resonance and a large disk radius. But the contribution by a small q is smaller than that by a small $\alpha_{\rm hot}$, since equation 2 shows the dependence of $t_{\rm d}$ to q is larger than that of α.

The fading rates of OT J075418 and OT J230425 were 0.0189(3) mag d^{-1} and 0.0340(4) mag d^{-1}, respectively. Figure 10 shows the relation between the superhump period in the stage B ($P_{\rm orb}$) and the fading rate of SU UMa-type DNe (filled circles), WZ Sge-type DNe (filled triangles) and possible candidates for the period bouncer including OT J075418 and OT J230425 (filled stars). SSS J122221 (J122221 in figure 10) was reported as a perfect candidate for the period bouncer (Kato et al. 2013b). Kato et al. (2013b) also suggests that OT J184228.1+483742 (J184228 in figure 10) showing double superoutburst is a good candidate for the period bouncer. According to figure 10, the fading rates of OT J075418 and OT J230418 are lower than those of SU UMa-type DNe with similar periods. Furthermore, the location of these objects is close to that of the good candidates for previously suggested the period bouncer. This strengthens the interpretation that these objects are good candidates for the period bouncer.

There are two objects near these candidates for the period bouncer in figure 10. One of them is BC Dor, which went through superoutburst in 2003, and another is PV Per detected its superoutburst in 2008. Their last superoutbursts were reported in Kato et al. (2009). Since they had relatively frequent outbursts, we considered them not to be candidates for the period bouncer. They were inside a range of the period bouncer in error in figure 10 due to the data of poor quality.

5.4. Absence of Early Superhumps

OT J184228, a likely candidate for the period bouncer, showed double superoutburst consisting of the first one with early superhumps and another one with ordinary superhumps (Kato et al. 2013b). SSS J122221 also showed the similar pattern of the superoutburst.

OT J075418 and OT J230425, however, showed no early superhumps. Early superhumps, as mentioned in section 1, arise when the disk radius reaches the 2:1 resonance radius due to its low q. And they cannot be detected in a system with a low inclination (e.g. GW Lib reported by Hiroi et al. 2009), since the origin of early superhumps is the emission of a disk surface that has a non-axisymmetric vertical structure (Nogami et al. 1997; Kato 2002). The absence of the stage of early superhumps may indicate that the radius of the 2:1 resonance was not reached in these objects. Although this generally does not support their low q, we expect OT J075418 and OT J230425 to have low q because of other strong evidence that we discussed

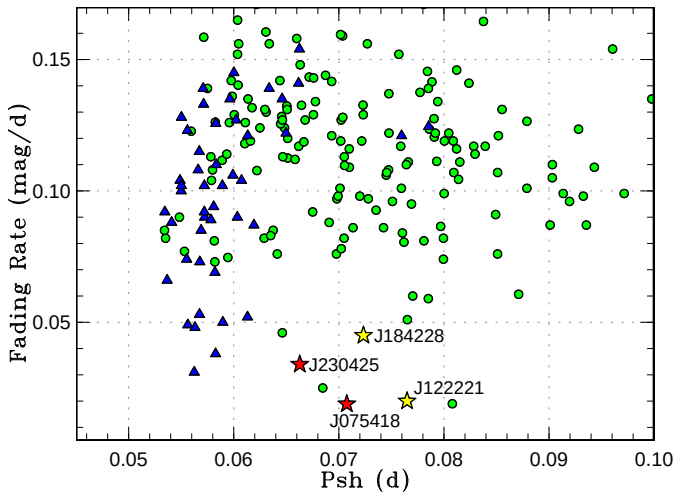

Fig. 10. Fading rate versus superhump period in the stage B. The data are from Kato et al. (2014a). The filled circles and the filled triangles represent SU UMa-type DNe and WZ Sge-type DNe, respectively. The filled stars represent the candidates for the period bouncer, including OT J075418 and OT J230425.

above. Furthermore, it has been reported that a system with corroborated low q did not show early superhumps (Kato et al. 2014b). It was considered that its superoutburst triggered by an inside-out (slowly rising) outburst made it impossible to establish the $2:1$ resonance.

5.5. Existence of a Precursor in OT J075418

In OT J075418, a precursor preceding the superoutburst was detected (BJD 2456325). This is rare in WZ Sge-type DNe, which hardly show a normal outburst.

Osaki, Meyer (2003) suggested that, in a superoutburst with a precursor the disk radius does not reach the tidal truncation radius, which is the maximum radius larger than the $3:1$ resonance, while the disk radius reaches the tidal truncation radius in a superoutburst without a precursor. It is thought that the system in a precursor fades rapidly as in a normal outburst, since its accretion disk does not reach the tidal truncation radius and the disk allows the cooling wave to propagate inward. During this fading, if the disk becomes sufficient eccentric, the tidal dissipation from the secondary brings the disk to the hot state. Then, it is observed as a superoutburst with a precursor. As mentioned in subsection 5.3, however, OT J075418 faded very slowly. Similarly, 1RXS J053234+624755 has a very small mass ratio 0.074(19) and showed a superoutburst with a precursor (Kapusta, Thorstensen 2006; Imada et al. 2009). Following Imada et al. (2009), we suggest that the radius of the accretion disk of OT J075418 should be far beyond the $3:1$ resonance, but not reach the tidal truncation radius, if a mass ratio of a system is small enough to make a sufficient space between the $3:1$ resonance and the tidal truncation radius.

As can be seen in the lightcurve, it took relatively a long time from fading of a precursor outburst to appearance of a superoutburst. It may be due to a long growth time of the $3:1$

resonance because of its small mass ratio.

5.6. Number Density Problem of Period Bouncers

Now, we know four candidates for the period bouncer (J075418, SSS J122221, OT J230425 and OT J184228). To investigate whether our observation is able to account for the missing population of period bouncers expected in the evolutionary theory, we counted how many superoutbursts of SU UMa stars were observed. In the recent five years, when the current project to observe SU UMa-type stars was undertaken in the same way as now, we have observed about 291 superoutbursts in 248 SU UMa-type stars (Kato et al. 2010; Kato et al. 2012; Kato et al. 2013a; Kato et al. 2014a). The number of detected superoutbursts is unknown[1].

The recurrence time of the superoutbursts $T_{\rm s}$ is inversely proportional to mass-transfer rate $\dot{M}$ (Osaki 1995) and $\dot{M}$ is approximately proportional to q^2 in a short-period system evolving by gravitational radiation (Patterson 1998). We can estimate the parent population of the period bouncers from the statistics of recorded outbursts. Since many of SU UMa-type DNe have $T_{\rm s} \sim 1$ yr, we can assume many of them have been detected in a superoutburst in the last five years. If the period bouncers have recurrence time of $T_{\rm s}$(PB), the detection probability of period bouncers can be estimated to be $5/T_{\rm s}({\rm PB}) \times f$, where f stands for fraction of time covered by surveys. If we conservatively assume $f \sim 0.1$–0.5, we can thus estimate the ratio of parent populations of $N({\rm PB})/N(\text{ordinary SU UMa-type}) \sim 4/248 \times 1/f \times T_{\rm s}({\rm PB})/5$.

There is large uncertainly in $T_{\rm s}$(PB). We can, however, estimate $T_{\rm s}({\rm PB}) > 5$ yr, since these objects were hardly detected in outbursts in the past CRTS and other surveys.[2] As to OT J230425, two outbursts have been detected by CRTS. One outburst was in 2006 December and the other was in 2011 January. It suggests that the recurrence time of the outbursts of OT J230425 is not as long as that of WZ Sge-type DNe. Therefore, it is possible that some candidates for the period bouncer have higher mass-transfer rate than we expected and go through outbursts more frequent than WZ Sge-type DNe. Three of the four candidates for the period bouncer are, however, WZ Sge-like stars. We assume that majority of the candidates for the period bouncer are WZ Sge-like stars and discuss the number density of period bouncers excluding the systems like OT J230425. We regard $N({\rm PB}) = 3$ hereafter, excluding OT J230425.

If we assume that the mass-transfer is purely driven by the gravitational wave radiation, $\dot{M}({\rm PB}) \sim 10^{-2}\dot{M}(\text{ordinary SU UMa-type})$ and $T_{\rm s}$(PB) is expected to be $\sim 10^2$ yr. If we assume $T_{\rm s}$(PB) is $\sim 10^1$ and $\sim 10^2$ yr and conservatively assume $f \sim 0.1$–0.5, we can obtain roughly $N({\rm PB})/N(\text{SU UMa}) \sim 0.24$–$12$. Considering the possibility of the period bouncers like OT

[1] There were systems that were detected its superoutburst but were not made time-series observations.

[2] Although typical intervals of observations in CRTS is 10 d, and there is a seasonal gap when the object is near the solar conjunction, we consider many (fraction f) of superoutburst should have been recorded since WZ Sge-type DNe usually show long-fading tails lasting several months. No previous outbursts in four systems suggest that $T_{\rm s}$ for these systems are efficiently long.

J230425, the population of the period bouncers can be estimated to be larger. As mentioned in section 1, it was predicted that the majority of CVs ($\sim 70\%$ by Kolb 1993) have passed the period bounce. On the contrary, few candidate for the period bouncer has been discovered by observations. We call theoretically predicted population of the period bouncer "the missing population" of the period bouncer. Although the true recurrence time of candidates for the period bouncer should be confirmed by future observations, this ratio suggests a possibility that the period bouncers we have identified can account for the missing population of the period bouncers expected from the evolutionary scenario. We thus identify these WZ Sge-type objects with unusual outburst properties are the good candidates for the hidden population of the terminal evolution of CVs.

Although we discussed photometric properties of the candidates for the period bouncer, Gänsicke et al. (2009) suggested their spectroscopic properties. They argued that SDSS CVs in the 80–86 min period spike showed spectra dominated by emission from the WD with no spectroscopic signature from the companion star at optical wavelengths. These characteristics suggest that these systems have very low accretion rates, and they are most likely DNe with extremely long recurrence time. It takes long time to detect many candidates for the period bouncer in photometric observations on account of their long recurrence time. Spectroscopic studies of the newly identified four candidates are desired.

6. Summary

We report on photometric observations of two dwarf novae, OT J075418.7+381225 and OT J230425.8+062546, which underwent superoutbursts in 2013 (OT J075418) and in 2011 (OT J230425). The results of the analysis of our data are summarized in table 1.

In OT J075418 and OT J230425, some peculiar properties that were similar to those of a good candidate for the period bouncer (SSS J122221.7−311523) could be seen. These two DNe are good candidates for the period bouncer. We then propose the general properties of candidates for the period bouncer as below:

- They show a very long growing stage of superhumps (stage A) and a large period decrease of the stage A-B transition ($\sim 1.5\%$). The long stage A, which reflects the slow evolution of the superhump, is due to the very small mass ratios of these objects.
- The decline rates in the plateau phase in the superoutburst of these objects are lower than those of SU UMa-type DNe with the similar superhump period to these objects.

To investigate whether our observation is able to account for the missing population of the period bouncers expected in the evolutionary theory, we counted how many SU UMa stars went through superoutbursts. In the recent five years, we have observed about 291 superoutbursts in 248 SU UMa-type stars and four good candidates for the period bouncer have been suggested, including OT J075418 and OT J230425. Three of four candidates were WZ Sge-

Table 1. The result of the analysis of OT J075418 and OT J230425.

	OT J075418	OT J230425
mean period*	0.0722403(26)	0.067317(35)
stage A†	0.072218(3)	0.067245(17)
	(56328–56341)	(55563–55572)
stage B‡	0.070758(6)	0.066351(12)
	(56345–56355)	(55571–55585)
fading rate§	0.0189(3)	0.0340(4)

*Mean period of the all superhumps. Unit d.

†Stage A superhump period. Unit d.
The intervals used to determine the periods are given in the parentheses. BJD−2400000.

‡Stage B superhump period. Unit d.
The intervals used to determine the periods are given in the parentheses. BJD−2400000.

§Unit mag d^{-1}.

like stars, and OT J230425 may have shorter recurrence time than the others. We estimated the number density of the period bouncers, excluding the systems like OT J230425. Although there is large uncertainty in the recurrence time of the period bouncers, we assumed superoutbursts of the period bouncers were 10^1–10^2 times more infrequent than those of ordinary SU UMa-type DNe, according to the theoretical prediction. Under this assumption, we can obtain roughly N(PB)/N(SU UMa)$\sim$ 0.24–12. This ratio suggests a probability that the period bouncers we have identified can account for the missing population of the period bouncers expected from the evolutionary scenario.

This work was supported by the Grant-in-Aid Initiative for High-Dimensional Data-Driven Science through Deepening of Sparse Modeling from the Ministry of Education, Culture, Sports, Science and Technology (MEXT) of Japan. We are grateful to many amateur observers for providing a lot of data used in this research.

References

Bailey, J. 1979, MNRAS, 189, 41P
Cleveland, W. S. 1979, J. Amer. Statist. Assoc., 74, 829
Downes, R. A. 1990, AJ, 99, 339
Drake, A. J., et al. 2009, ApJ, 696, 870
Fernie, J. D. 1989, PASP, 101, 225
Gänsicke, B. T., et al. 2009, MNRAS, 397, 2170

Table 2. Log of observations of OT J075418.

Start*	End*	mag†	error‡	N§	obs‖	sys#
25.2913	25.4934	15.947	0.003	229	deM	C
26.2986	26.6882	16.191	0.010	489	deM	C
27.2431	27.6752	15.120	0.003	433	MEV	C
27.2980	27.6668	14.983	0.003	460	deM	C
27.6840	27.9237	14.944	0.003	286	GFB	C
28.2990	28.6527	14.923	0.001	441	deM	C
28.5383	28.7812	14.988	0.002	290	DKS	C
28.7016	28.9420	14.884	0.001	585	SWI	V
29.2968	29.6605	14.969	0.001	514	deM	C
29.6677	29.8488	15.019	0.002	200	GFB	C
29.7057	29.9564	14.881	0.001	609	SWI	V
30.2980	30.6371	15.005	0.001	500	deM	C
30.7285	30.9638	14.909	0.001	572	SWI	V
31.3028	31.6423	15.050	0.001	502	deM	C
31.7016	31.9142	14.968	0.001	364	SWI	V
32.3015	32.6886	15.105	0.001	608	deM	C
32.3054	32.6595	15.138	0.001	355	MEV	C
33.3011	33.6583	15.175	0.001	354	MEV	C
36.5681	36.5681	15.180	–	1	MUY	C
36.6996	36.9058	1.169	0.001	353	SWI	C
36.6996	36.9058	15.198	0.001	353	SWI	V
37.6966	37.8978	1.166	0.001	345	SWI	C
38.3036	38.6830	15.270	0.001	468	CDZ	C
39.3021	39.5805	15.299	0.002	308	CDZ	C
39.3564	39.6420	15.347	0.001	256	MEV	C

*BJD−2456300.

†Mean magnitude.

‡1-σ of the mean magnitude.

§Number of observations.

‖Observer's code. deM (E. de Miguel), MEV (E. Morelle), GFB (W. Goff), DKS (S. Dvorak), SWI (W. Stein), MUY (E. Muyllaert), CDZ (AAVSO data), DPV (P. Dubovsky)

#Filter. "C" means no filter (clear).

Table 2. Log of observations of OT J075418 (continued).

Start*	End*	mag†	error‡	N§	obs‖	sys#
40.3004	40.6396	15.386	0.002	251	MEV	C
40.3940	40.6534	15.346	0.002	293	CDZ	C
46.3199	46.4654	15.350	0.003	148	MEV	C
47.4372	47.6331	15.362	0.002	207	deM	C
48.4312	48.6151	15.415	0.002	232	deM	C
49.4269	49.6170	15.449	0.003	212	deM	C
50.4413	50.5910	15.499	0.002	182	deM	C
52.2781	52.5203	2.233	0.005	281	DPV	C
53.3085	53.5875	15.658	0.002	354	deM	C
54.2581	54.4964	2.554	0.003	300	DPV	C
54.3650	54.6011	15.740	0.002	184	MEV	C
56.2530	56.5597	2.655	0.002	386	DPV	C
57.2314	57.5306	2.781	0.002	360	DPV	C

*BJD−2456300.

†Mean magnitude.

‡1-σ of the mean magnitude.

§Number of observations.

‖Observer's code. deM (E. de Miguel), MEV (E. Morelle), GFB (W. Goff), DKS (S. Dvorak), SWI (W. Stein), MUY (E. Muyllaert), CDZ (AAVSO data), DPV (P. Dubovsky)

#Filter. "C" means no filter (clear).

Hiroi, K., et al. 2009, PASJ, 61, 697

Imada, A., et al. 2009, PASJ, 61, L17

Kapusta, A. B., & Thorstensen, J. R. 2006, PASP, 118, 1119

Kato, T. 2002, PASJ, 54, L11

Kato, T., et al. 2013a, PASJ, 65, 23

Kato, T., et al. 2014a, PASJ, 66, 30

Kato, T., et al. 2009, PASJ, 61, S395

Kato, T., & Maehara, H. 2013, PASJ, 65, 76

Kato, T., et al. 2012, PASJ, 64, 21

Kato, T., et al. 2010, PASJ, 62, 1525

Kato, T., Monard, B., Hambsch, F.-J., Kiyota, S., & Maehara, H. 2013b, PASJ, 65, L11

Kato, T., et al. 2014b, PASJ, in press (arXiv/1407.4196)

Kato, T., & Osaki, Y. 2013, PASJ, 65, 115

Kato, T., Sekine, Y., & Hirata, R. 2001, PASJ, 53, 1191

Table 3. Log of observations of OT J230425.

Start*	End*	mag†	error‡	N§	obs‖	sys#
63.9532	64.0147	13.775	0.005	130	Siz	C
65.8770	65.9577	14.149	0.004	146	Mhh	C
65.8827	65.9319	13.683	0.005	107	Ioh	C
65.8902	66.0023	13.783	0.002	224	Siz	C
67.8853	68.0198	13.871	0.005	264	Siz	C
68.8860	69.0162	13.876	0.004	259	Siz	C
68.9449	69.0041	13.887	0.008	132	Ioh	C
68.9769	68.9841	14.259	0.019	16	Mhh	C
69.8702	70.0000	13.879	0.006	280	Ioh	C
69.8802	69.9934	14.217	0.004	424	Mhh	C
69.8892	70.0194	13.918	0.007	231	Siz	C
70.8707	71.0046	13.908	0.007	268	Ioh	C
71.8613	71.9994	13.851	0.005	292	Ioh	C
71.8624	72.0124	13.848	0.006	299	Siz	C
72.1643	72.2480	14.044	0.022	29	CRI	C
73.1712	73.2678	13.813	0.008	47	CRI	C
73.9053	73.9859	14.018	0.016	132	Ioh	C
73.9302	74.0088	14.028	0.016	120	Siz	C
74.8823	74.9998	13.951	0.009	236	Siz	C
75.1832	75.2627	13.920	0.012	26	CRI	C
75.8838	75.9353	14.272	0.009	182	Mhh	C
75.9042	75.9720	13.962	0.006	134	Siz	C
78.8920	78.9520	14.094	0.007	122	Siz	C
78.9242	78.9722	14.508	0.008	182	Mhh	C
79.9057	79.9786	14.275	0.015	120	Siz	C
80.8940	80.9777	14.449	0.022	166	Siz	C
80.9083	80.9452	14.588	0.009	136	Mhh	C
83.8728	83.9645	14.549	0.016	158	Ioh	C
86.9111	86.9111	17.401	–	1	Siz	C

*BJD−2455500.

†Mean magnitude.

‡1-σ of the mean magnitude.

§Number of observations.

‖Observer's code. Siz (K. Shiokawa), Mhh (H. Maehara), Ioh (H. Itoh), CRI (Crimean Astrophys. Obs.)

#Filter. "C" means no filter (clear).

Table 4. Times of superhump maxima in OT J075418.

E	max*	error	$O-C^{\dagger}$	$N^{\ddagger}$
0	56325.4119	0.0040	−0.0295	65
13	56326.3502	0.0065	−0.0224	72
14	56326.4264	0.0018	−0.0179	73
15	56326.4975	0.0013	−0.0184	71
16	56326.5656	0.0019	−0.0219	72
17	56326.6432	0.0020	−0.0160	74
26	56327.2791	0.0005	−0.0249	64
27	56327.3527	0.0005	−0.0229	136
28	56327.4234	0.0004	−0.0238	138
29	56327.4965	0.0008	−0.0224	125
30	56327.5678	0.0004	−0.0227	106
31	56327.6370	0.0005	−0.0251	139
32	56327.7092	0.0004	−0.0246	62
33	56327.7832	0.0010	−0.0222	64
34	56327.8537	0.0007	−0.0233	71
35	56327.9219	0.0023	−0.0268	44
41	56328.3564	0.0007	−0.0221	73
42	56328.4308	0.0007	−0.0193	73
43	56328.4955	0.0009	−0.0263	71
44	56328.5700	0.0008	−0.0234	138
45	56328.6443	0.0011	−0.0208	123
46	56328.7130	0.0010	−0.0236	157
47	56328.7840	0.0005	−0.0243	178
48	56328.8524	0.0006	−0.0275	141
49	56328.9284	0.0010	−0.0232	115
55	56329.3637	0.0029	−0.0177	87
56	56329.4315	0.0012	−0.0216	83
57	56329.5031	0.0023	−0.0215	82
58	56329.5719	0.0013	−0.0244	83
59	56329.6463	0.0016	−0.0216	61
60	56329.7189	0.0007	−0.0207	158

*BJD−2400000.

†$C = 2456325.4414 + 0.0716368E$.

‡Number of points used to determine the maximum.

Table 4. Times of superhump maxima in OT J075418 (continued).

E	max*	error	$O-C^{\dagger}$	$N^{\ddagger}$
61	56329.7986	0.0014	−0.0126	198
62	56329.8692	0.0013	−0.0137	157
63	56329.9355	0.0017	−0.0190	133
69	56330.3692	0.0015	−0.0151	85
70	56330.4385	0.0011	−0.0174	84
71	56330.5183	0.0014	−0.0092	86
72	56330.5836	0.0010	−0.0156	89
74	56330.7380	0.0024	−0.0045	78
75	56330.8028	0.0009	−0.0113	140
76	56330.8767	0.0007	−0.0091	141
77	56330.9376	0.0011	−0.0198	141
83	56331.3822	0.0019	−0.0050	80
84	56331.4572	0.0011	−0.0017	77
85	56331.5234	0.0014	−0.0071	95
86	56331.5895	0.0028	−0.0126	94
88	56331.7528	0.0020	0.0074	99
89	56331.8094	0.0018	−0.0077	99
90	56331.8869	0.0022	−0.0018	99
97	56332.4002	0.0027	0.0100	158
98	56332.4612	0.0018	−0.0006	145
99	56332.5408	0.0021	0.0074	154
100	56332.6046	0.0018	−0.0004	152
101	56332.6660	0.0058	−0.0107	127
110	56333.3244	0.0012	0.0030	45
111	56333.3999	0.0008	0.0068	59
112	56333.4755	0.0022	0.0108	61
113	56333.5443	0.0027	0.0080	54
114	56333.6192	0.0008	0.0112	61
157	56336.7342	0.0008	0.0459	188
158	56336.7965	0.0006	0.0365	198
159	56336.8676	0.0013	0.0359	196
171	56337.7416	0.0011	0.0504	99
172	56337.8029	0.0012	0.0400	99

*BJD−2400000.

†$C = 2456325.4414 + 0.0716368E$.

‡Number of points used to determine the maximum.

Table 4. Times of superhump maxima in OT J075418 (continued).

E	max*	error	$O-C^{\dagger}$	$N^{\ddagger}$
179	56338.3237	0.0015	0.0593	51
180	56338.3865	0.0013	0.0505	71
181	56338.4648	0.0013	0.0572	70
182	56338.5365	0.0010	0.0572	71
183	56338.6070	0.0018	0.0561	72
193	56339.3314	0.0025	0.0641	74
194	56339.4109	0.0011	0.0720	73
195	56339.4686	0.0017	0.0580	131
196	56339.5543	0.0045	0.0721	136
197	56339.6130	0.0009	0.0592	69
207	56340.3481	0.0020	0.0779	55
208	56340.4063	0.0029	0.0645	91
209	56340.4856	0.0013	0.0722	123
210	56340.5570	0.0020	0.0719	89
211	56340.6249	0.0013	0.0681	91
291	56346.3452	0.0008	0.0575	47
292	56346.4170	0.0007	0.0576	56
307	56347.4816	0.0011	0.0478	50
308	56347.5504	0.0015	0.0449	61
309	56347.6214	0.0020	0.0442	49
321	56348.4747	0.0011	0.0379	71
322	56348.5453	0.0018	0.0368	70
335	56349.4669	0.0012	0.0272	70
336	56349.5385	0.0013	0.0272	46
337	56349.6049	0.0017	0.0220	59
376	56352.3683	0.0014	−0.0085	70
390	56353.3551	0.0011	−0.0246	72
391	56353.4255	0.0011	−0.0258	70
392	56353.4981	0.0012	−0.0249	72
393	56353.5691	0.0010	−0.0256	63

*BJD−2400000.

†$C = 2456325.4414 + 0.0716368E$.

‡Number of points used to determine the maximum.

Table 4. Times of superhump maxima in OT J075418 (continued).

E	max*	error	$O-C^{\dagger}$	$N^{\ddagger}$
404	56354.3470	0.0012	−0.0357	74
405	56354.4204	0.0021	−0.0339	99
406	56354.4874	0.0009	−0.0385	105
407	56354.5571	0.0010	−0.0404	55
432	56356.3251	0.0020	−0.0633	71
433	56356.3984	0.0031	−0.0617	72
434	56356.4674	0.0014	−0.0643	70
435	56356.5428	0.0012	−0.0606	61
446	56357.3150	0.0016	−0.0764	67
447	56357.3838	0.0018	−0.0793	67
448	56357.4591	0.0013	−0.0756	70

*BJD−2400000.

†$C = 2456325.4414 + 0.0716368E$.

‡Number of points used to determine the maximum.

Kato, T., & Uemura, M. 2012, PASJ, 64, 122

Knigge, C., Baraffe, I., & Patterson, J. 2011, ApJS, 194, 28

Kolb, U. 1993, A&A, 271, 149

Littlefair, S. P., Dhillon, V. S., Marsh, T. R., Gänsicke, B. T., Southworth, J., Baraffe, I., Watson, C. A., & Copperwheat, C. 2008, MNRAS, 388, 1582

Littlefair, S. P., Dhillon, V. S., Marsh, T. R., Gänsicke, B. T., Southworth, J., & Watson, C. A. 2006, Science, 314, 1578

Lubow, S. H. 1991, ApJ, 381, 259

Lubow, S. H. 1992, ApJ, 398, 525

Murray, J. R. 2000, MNRAS, 314, L1

Nakano, S., Nishimura, H., Kadota, K., & Yusa, T. 2011, Cent. Bur. Electron. Telegrams, 2616

Nakata, C., et al. 2013, PASJ, 65, 117

Nogami, D., Kato, T., Baba, H., Matsumoto, K., Arimoto, J., Tanabe, K., & Ishikawa, K. 1997, ApJ, 490, 840

Osaki, Y. 1989, PASJ, 41, 1005

Osaki, Y. 1995, PASJ, 47, 47

Osaki, Y., & Kato, T. 2013, PASJ, 65, 50

Osaki, Y., & Meyer, F. 2003, A&A, 401, 325

Patterson, J. 1998, PASP, 110, 1132

Patterson, J. 2011, MNRAS, 411, 2695

Patterson, J., et al. 1998, PASP, 110, 1290

Stellingwerf, R. F. 1978, ApJ, 224, 953

Table 5. Times of superhump maxima in OT J230425.

E	max*	error	$O-C^{\dagger}$	$N^{\ddagger}$
0	55563.9791	0.0028	−0.0354	108
29	55565.9214	0.0011	−0.0273	274
30	55565.9956	0.0023	−0.0198	64
59	55567.9479	0.0017	−0.0019	104
60	55568.0077	0.0015	−0.0087	70
74	55568.9571	0.0016	0.0069	215
88	55569.8972	0.0014	0.0132	347
89	55569.9608	0.0018	0.0101	427
103	55570.9046	0.0013	0.0201	116
104	55570.9694	0.0011	0.0182	107
118	55571.9022	0.0009	0.0172	217
119	55571.9743	0.0014	0.0226	211
122	55572.1788	0.0022	0.0271	15
123	55572.2380	0.0014	0.0195	12
137	55573.1684	0.0071	0.0162	16
149	55573.9517	0.0014	−0.0009	148
164	55574.9499	0.0013	−0.0032	107
179	55575.9383	0.0022	−0.0153	150
224	55578.9187	0.0043	−0.0364	237
254	55580.9340	0.0014	−0.0221	192

*BJD−2400000.

†$C = 2455565.925 + 0.06695E$.

‡Number of points used to determine the maximum.